Biomatter 3:3, e24648; July/August/September 2013; © 2013 Landes Bioscience

Progressive alterations in microstructural organization and biomechanical response in the ApoE mouse model of aneurysm

Darren Haskett,[1] Mohamad Azhar,[2] Urs Utzinger[1,3,4] and Jonathan P. Vande Geest[1,3-5,*]

[1]Graduate Interdisciplinary Program of Biomedical Engineering; University of Arizona; Tucson, AZ USA; [2]Developmental Biology and Neonatal Medicine Program, Herman B. Wells Center for Pediatric Research, Indiana University School of Medicine, Indianapolis, IN USA; [3]BIO5 Institute; University of Arizona; Tucson, AZ USA; [4]Department of Biomedical Engineering; University of Arizona; Tucson, AZ USA; [5]Department of Aerospace and Mechanical Engineering; University of Arizona; Tucson, AZ USA

Keywords: ApoE, AAA, Aneurysm, mouse model, mechanical, microstructure, two-photon, AngII

AAA is a complex disease that leads to a localized dilation of the infrarenal aorta that develops over years. Longitudinal information in humans has been difficult to obtain for this disease, therefore mouse models have become increasingly used to study the development of AAAs. The objective of this study was to determine any changes that occur in the biomechanical response and fiber microstructure in the ApoE$^{-/-}$ AngII mouse model of aneurysm during disease progression. Adult ApoE$^{-/-}$ AngII infused mice along with wild-type controls were taken at 14 and 28 d. Aortas were excised and tested simultaneously for biaxial mechanical response and ECM organization. Data sets were fit to a Fung-type constitutive model to give peak strains and stiffness values. Images from two photon microscopy were quantified in order to assess the preferred fiber alignment and degree of fiber orientation. Biomechanical results found significant differences that were present at 14 d had returned to normal by 28 d along with significant changes in fiber orientation and dispersion indicating remodeling occurring within the aneurysmal wall. This return of some of the normal biomechanical function, in addition the continuing changes that occur in the microstructure suggest a restorative response that occurs in the ApoE$^{-/-}$ AngII infused model after the initial aneurysm formation.

Introduction

Abdominal aortic aneurysm (AAA) is currently a leading cause of death in developed countries with occurrence rates expected to increase with aging populations.[1] As they are often asymptomatic, once rupture occurs, AAA is associated with significant morbidity and mortality. Studies have shown that aneurysmal tissue is remodeled in the disease process in humans with alterations in mechanical properties.[2,3] However, AAA disease is complex and develops over years and obtaining longitudinal information from patients has proven very difficult, thus making the study of the underlying mechanisms of disease initiation and progression problematic. To redress this lack of knowledge involving the evolving mechanical properties with the physiological processes, mouse models have become increasingly used to study the development of AAAs.

Prominent among these mouse models for aneurysm is the apolipoprotein-E knockout (ApoE$^{-/-}$) mouse with long-term subcutaneous infusion of angiotensin II (AngII) described by Daugherty et al.[4] Recently several publications have considered the ApoE$^{-/-}$ AngII infused model of AAA looking at causes of inflammation and inhibiting aneurysm formation.[5-8] While important, such studies do not provide insight into the hemodynamics or mechanical environment which are now considered instigating factors in the initiation and progression of disease. To fill this gap in the literature, recent work by Ford[9] and Goergen[10] have looked into the hemodynamics and cyclic strain in the ApoE$^{-/-}$ AngII infused model of AAA, respectively.

Still missing, though, are the biomechanical properties of the ApoE$^{-/-}$ AngII infused model of AAA associated with progression of disease. Also of importance, is the need to couple any biomechanical modeling with changes in extracellular matrix and associated alterations in microstructure. Recent work has started to address this by first defining the mechanical properties and constitutive modeling of wild-type (C57BL/6) mice.[11,12] However, these studies do not include the actual the ApoE$^{-/-}$ AngII infused model of AAA. The purpose of this paper is to assess changes that occur in the biomechanical response along with associated ECM remodeling and alterations in fiber response during disease progression for the ApoE$^{-/-}$ AngII infused mouse model of AAA.

Results

General response. As anticipated there was no difference found in any metric between the two time periods of 14 and 28 d for

*Correspondence to: Jonathan P. Vande Geest; Email: jpv1@email.arizona.edu
Submitted: 03/31/13; Accepted: 04/08/13
Citation: Haskett D, Azhar M, Utzinger U, Vande Geest J. Progressive alterations in microstructural organization and biomechanical response in the ApoE mouse model of aneurysm. Biomatter 2013; 3:e24648; PMID: 23628871; http://dx.doi.org10.4161/biom.24648.

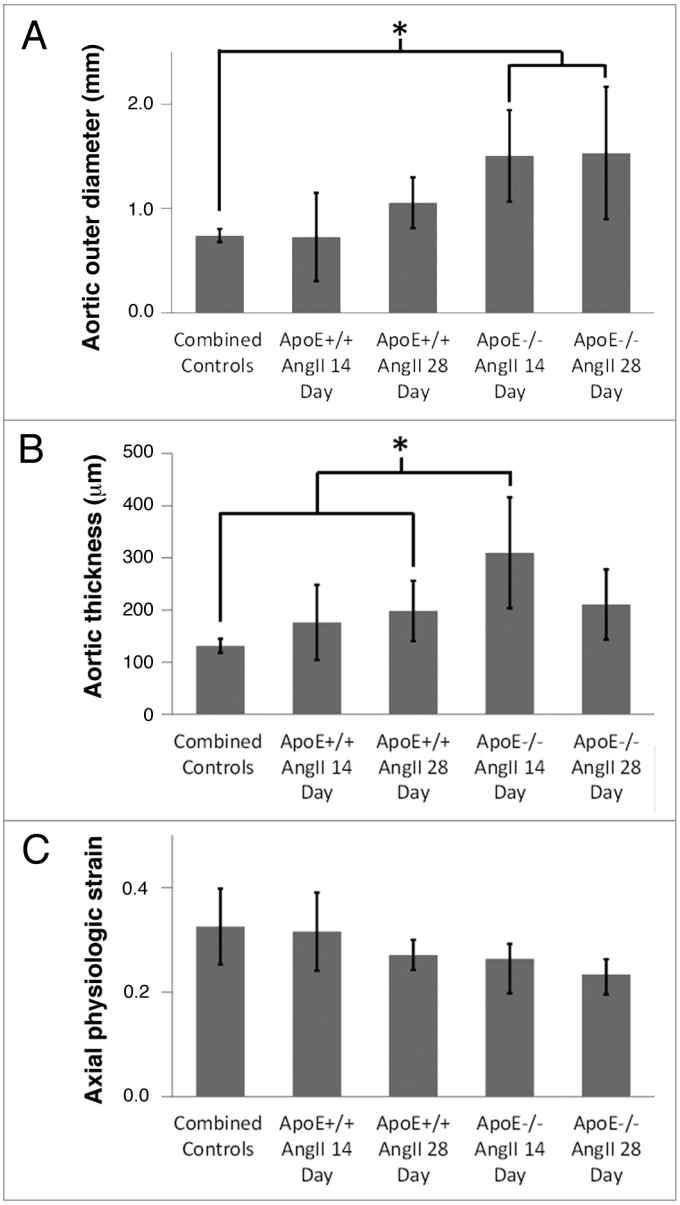

Figure 1. (**A**) The initial unloaded outer diameter of the suprarenal segment of the aorta tested taken at its greatest point. (**B**) The initial undeformed thickness of the suprarenal segment of the aorta taken adjacent to the section tested. (**C**) The physiologic strain measured prior to mechanical testing. Error bars shown are standard deviation (*$p < 0.05$).

the control mice, thus the data have been combined into one group for reporting below. General results include the significant increase in outer aortic diameter for both 14 and 28 d groups of the aneurysmal ApoE$^{-/-}$ AngII infused model compared with controls (**Fig. 1A**). The 14 d ApoE$^{-/-}$ AngII infused model aneurysmal group was found to be significantly greater than controls as well as wild-type AngII infused groups, however the 28 d ApoE$^{-/-}$ AngII infused group was not significantly different from controls or wild-type AngII infused groups (**Fig. 1B**). Although physiologic strain tended to decrease with both AngII infusion and with time and more so with the ApoE$^{-/-}$ AngII infused model, there were no significant differences found among the groups (**Fig. 1C**).

Mechanics and constitutive relationship. Parameters for each individual constitutive fit can be found in **Table 1**. There was a significant decrease in circumferential strain at both time points in the ApoE$^{-/-}$ AngII infused aneurysmal model (**Fig. 2A**). This decrease in circumferential strain was accompanied by an increase in circumferential stiffness, however, the aneurysmal model was not found to be significantly different from the controls or AngII infused wild-type mice due to the high variability (**Fig. 2B**). The axial stiffness tended to decrease with 14 d of AngII infusion for both wild-type and ApoE$^{-/-}$ mice, but then return closer to the stiffness found in the control mice after 28 d of AngII infusion (**Fig. 2C**). The axial stiffness was significantly higher than the circumferential stiffness for both the control and AngII infused wild-type mice groups, but this was not the case for either time point in the ApoE$^{-/-}$ AngII infused aneurysmal model.

Fiber alignment. SHG imaging showed differences in the collagen structure between the control mice and the ApoE$^{-/-}$ AngII infused aneurismal mice at both 14 and 28 d time points (**Fig. 3**). Images show differences in the characteristic collagen crimp that is present in the control images before and during pressurization, which appears to be absent or greatly reduced in the ApoE$^{-/-}$ AngII infused aneurysm model. Representative histograms depicting the fiber angles compiled from each image stack at each pressurization (**Fig. 4**) demonstrate a response in fiber orientation and dispersion occurred with pressurization for controls that was absent at both time points in the ApoE$^{-/-}$ AngII infused aneurysm model.

The histograms were used to determine fiber orientation mean mode and FWHM. From the FWHM (**Fig. 5A**), the control mice showed a significant increase in fiber dispersion between 0 and 100 mmHg pressurization. An increase nearing significance also occurred in fiber dispersion for the 14 d AngII infused wild-type mice, but was absent in the 28 d AngII infused wild-type mice. The FWHM of ApoE$^{-/-}$ AngII aneurysmal mice at both time points did not express a significant change with pressurization, and at 0 mmHg the FWHM of the 28 d ApoE$^{-/-}$ AngII infused aneurysmal mice was significantly greater than control mice. The fiber directionality given by the mean mode (**Fig. 5B**) showed a more axial alignment for control mice that shifted significantly toward axial alignment with pressurization, this axial shift also occurred for AngII infused wild-type mice at both 14 and 28 d time points, though it was not significant. The shift with pressurization tended to be reversed for the ApoE$^{-/-}$ AngII aneurysmal mice at 14 d, and absent at 28 d. Also for the ApoE$^{-/-}$ AngII aneurysmal mice at 28 d, the preferred axial alignment similarly reduced or absent.

Cross sectional images (**Fig. 6**) illustrate the dissected aneurysmal sac that occurs in the ApoE$^{-/-}$ AngII aneurysmal model compared with control mice. ApoE$^{-/-}$ AngII aneurysmal images also reveal the elastic bands that appear to remain intact for all groups, while exhibiting adventitial thickening occurring with aneurysm and increased collagen content for the 28 d ApoE$^{-/-}$ AngII aneurysmal mice.

Discussion

A summary of the results found that as one would expect, the aortic outer diameter of the aneurysmal model was significantly greater than controls. However, this increase only translated to a significant increase in aortic thickness for the 14 d ApoE$^{-/-}$ AngII infused aneurysmal mice and not to the 28 d ApoE$^{-/-}$ AngII infused aneurysmal mice suggesting that remodeling within the aortic aneurysmal wall is occurring between 14 and 28 d. This remodeling between 14 and 28 d in the aneurysmal model is also suggested by the change in axial stiffness that occurred between 14 and 28 d in the ApoE$^{-/-}$ AngII infused aneurysmal mice, as there was initially a decrease in axial stiffness that was approaching significance, yet at 28 d ApoE$^{-/-}$ AngII infused aneurysmal mice had axial stiffness values closer to those found in the control mice. This trend in decreased axial stiffness at 14 d which was then corrected at 28 d was also found to occur with AngII infusion of wild-type mice suggesting a response not just to aneurysm formation but also AngII indused remodeling as well. One difference that was found, though, between controls and AngII infused wild-type mice compared with the ApoE$^{-/-}$ AngII infused aneurysmal model present at both 14 and 28 d time points was the decrease in circumferential strain and increase in circumferential stiffness.

Multiphoton images showed alterations in fiber appearance in the ApoE$^{-/-}$ AngII infused aneurysmal model and a loss of the characteristic crimp seen in collagen fiber bundles. Both metrics of fiber angle mean mode and FWHM showed gross changes between control and ApoE$^{-/-}$ AngII infused aneurysmal mice. While the control mice were able to respond with increases in fiber dispersion and shifts in mean fiber angle in the direction of increased stress, the ApoE$^{-/-}$ AngII infused aneurysmal mice lacked this ability. Thus, changes in the ApoE$^{-/-}$ AngII infused aneurysmal mice fiber structure and composition between time points appear to be compensation to the loss in function and ability to respond with shifts in mean fiber angle and dispersion to pressurization.

The ApoE$^{-/-}$ AngII mouse model of aneurysm has become a standard animal model for aneurysm with a plethora of papers just released within the past year examining multiple factors involved with AAA formation, progression, or prevention,[5-8,13,14] and while many other recent papers examining the biology of AAA disease often implicate mechanics as being a factor,[15-17] the biaxial properties of the ApoE$^{-/-}$ AngII aneurysmal aorta had yet to be examined until now. While previous studies in our lab[12] and other others such as Collins et al.[11] and Fujikura et al.[18] have used wild-type C57BL/6 mice to look into the mechanical properties of the mouse aorta to gain a more complete picture of underlying properties of vessel response, these studies did not include specimens from the actual ApoE AngII infused aneurysm model. And although Collins et al. reported some histology, absent in both their work and that of Fujikura et al. is analysis of fiber microstructure simultaneously with biomechanical response.

One limitation of the study was the inherent uncertainty of the aortic thickness from which the mechanical results were determined, especially for the aneurysmal specimens as the wall thickness varied around perimeter of the aneurysm due to the dissection creating thicker regions which then had to be averaged. Also, thickness measurements were made from an annulus taken adjacent to the region tested, and although these still included aneurysmal portions of the ApoE$^{-/-}$ AngII infused mice, some imprecision may have been introduced. Also, use of a Fung-type exponential constitutive model comes with limitations such as a lack of ability to capture multiple convexities and can result in constitutive parameters that are not unique.[2,19]

Another limitation of the study included the tubular imaging of aneurysmal specimens being unable to penetrate through the entire thickness of the aortic wall. Even though multiphoton imaging offers advantages for deep tissue imaging, there was still significant signal loss deeper into the tissue, so that image stacks

Table 1. Fung constants fit to the experimental data of control, AngII infused wild-type mice, and ApoE$^{-/-}$ AngII infused model, along with corresponding R^2 values

	C_0 (kPa)	a_1	a_2	a_{12}	R_2
Controls					
a	366.9	0.165	2.187	3.26E−02	0.97
b	229.6	0.225	4.879	1.67E−09	0.97
c	681.6	0.229	2.078	2.60E−02	0.99
d	123.6	0.0566	7.630	3.78E−01	0.95
e	128.8	0.480	5.445	1.86E−10	0.90
f	1713.3	0.00523	0.0607	2.22E−03	0.93
g	2391.0	0.0750	0.285	1.37E−02	0.97
h	5482.5	0.0328	0.115	4.43E−03	0.98
ApoE$^{+/+}$ AngII 14 d					
a	3838.0	0.0301	0.113	7.10E−04	0.96
b	2285.2	0.0328	0.213	1.90E−03	0.98
c	1297.7	1.17E−09	1.129	4.23E−02	0.95
d	5915.0	0.0243	0.123	2.51E−03	0.98
ApoE$^{+/+}$ AngII 28 d					
a	240.2	0.206	2.078	1.99E−02	0.91
b	886.8	0.177	0.409	4.20E−03	0.95
c	231.8	0.319	2.854	3.22E−10	0.98
d	200.9	0.437	3.185	1.03E−09	0.98
ApoE$^{-/-}$ AngII 14 d					
a	12.9	9.245	12.802	3.60E−01	0.85
b	356.2	1.900	0.881	4.90E−01	0.84
c	554.1	0.271	0.353	0.000714	0.96
ApoE$^{-/-}$ AngII 28 d					
a	11.2	12.317	19.74	8.05E+01	0.95
b	174.7	0.233	1.254	1.02E−09	0.95
c	297.2	4.865	1.556	7.43E−01	0.73

Descriptions for the material parameters are in "Data analysis and constitutive framework."

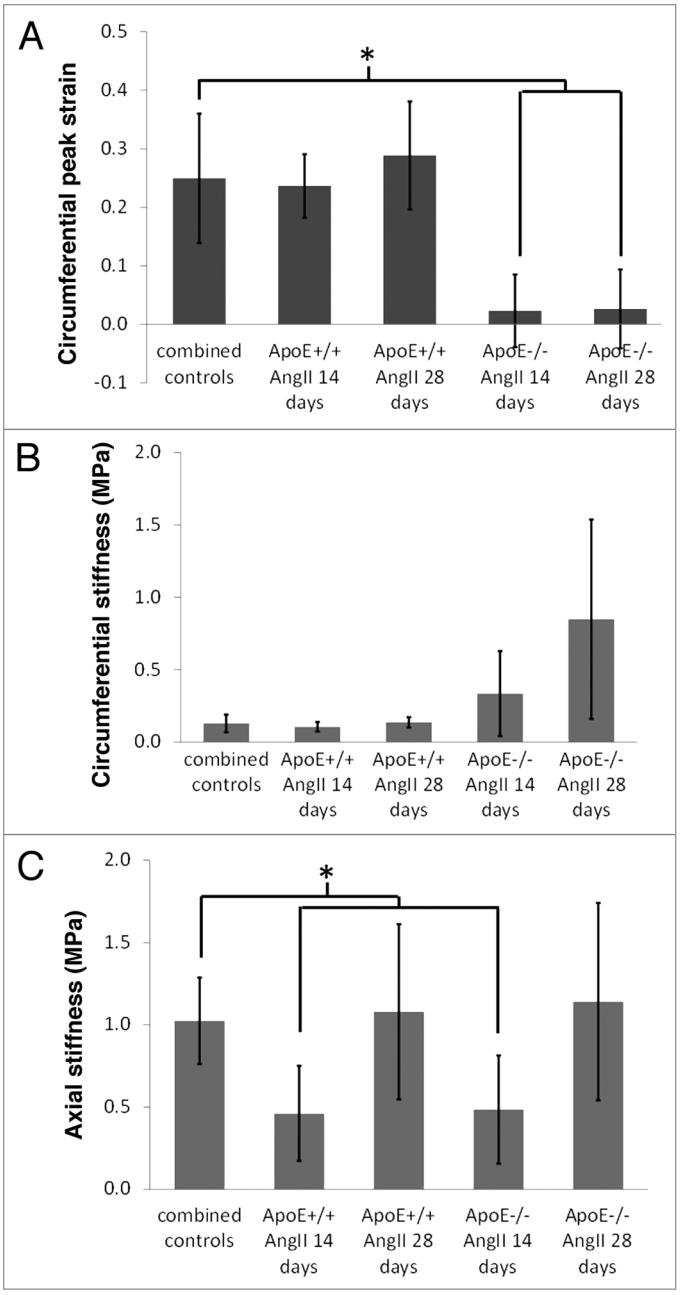

Figure 2. (**A**) The circumferential peak strain taken at the physiologic axial strain and pressurized to 100 mmHg. (**B and C**) The circumferential stiffness and axial stiffness, respectively, defined as $\partial S/\partial E$ in the circumferential and axial directions at the physiologic axial strain and peak circumferential strain. Error bars shown are standard deviation (*$p < 0.05$).

were kept to only 100 μm from the outside of the adventitia moving toward the media for analysis. However, while most imaging of mouse vascular walls has been conducted using cross-sectional imaging,[20-22] tubular imaging is still preferable to cross-sectional imaging in order to evaluate collagen fiber structure that would not be visible in any other plane. Additionally, full cross-sectional images were unable to be obtained from all specimens. However, cross-sectional images that were able to be obtained suggest that much of the remodeling that occurred between the 14 and 28 d time points in the ApoE$^{-/-}$ AngII infused aneurysm model was primarily collagen remodeling and occurred in the adventitia and the intraluminal thrombus, a finding supported by Schriefl et al.[21] Thus, focusing our study on the collagen remodeling occurring in the adventitia though tubular imaging is appropriate in this case.

Future work focusing on the collagen fiber remodeling could be improved by implementing a constitutive model that includes fiber directionality such as that used by Collins et al.[11] or other more microstructurally based constitutive relationships.[23,24] Such microstructurally based constitutive relationships could also help when comparisons are made between different aneurysm models and the human disease. One thing that our work here has indicated is that there seems to be response in the ApoE$^{-/-}$ AngII infused model by 28 d that is able to reverse some of the functional mechanical response lost at 14 d. This is similar to findings by Daugherty et al.,[25] which showed through histology that after 84 d of AngII infusion there was considerable remodeling of aneurysmal tissue with thinning regions not found at 28 d. We know that this late stage response is happening in the ApoE$^{-/-}$ AngII mouse model and this does not happen in the human disease, so beyond a certain time point, the model may not be useful or appropriate for studying the human disease. Other authors have also found differences between the ApoE$^{-/-}$ AngII infused model and the human disease, such as Saraff et al.,[26] who found aortic dissection is a preceding factor in aneurysm formation in the ApoE$^{-/-}$ AngII infused model. Additionally, Schrifl et al.[21] found remodeling and fibrosis of the intraluminal thrombus in the ApoE$^{-/-}$ AngII infused model which could account for some of the recovered mechanical response. However, this does not mean that measurements taken at time of initial aneurysm formation may not be valuable in studying AAA.

Methods

Mouse model and specimen preparation. ApoE knockout mice (*ApoE*$^{-/-}$) were bred from stock obtained from The Jackson Laboratory, backcrossed 10 times into wild-type C57BL/6J background, and maintained as a colony of heterozygous animals. All animal use and experimental procedures for mouse testing were performed according to the approved protocol (#06-045) of the University of Arizona Institutional Animal Care and Use Committee (IACUC) and Animal Welfare Assurance Number (A3248-01). Adult (approximately six month old) *ApoE*$^{-/-}$ and *ApoE*$^{+/+}$ (C57BL/6J wild-type control mice) had Azlet® miniosmotic pumps (Durect Corp) implanted subcutaneously into the dorsum under anesthesia. Pumps were filled with either AngII (Sigma-Aldrich) to provide for continuous infusion at a rate of 1,000 ng/kg/min or saline for either 14 or 28 d (models 2002 and 2004 respectively) as described in the literature.[15,27,28] Mice were placed on a high fat diet and fed ad libitum. Groups included control mice with saline vehicle (n = 8), control mice with AngII vehicle (n = 8), and the aneurysm model of *ApoE*$^{-/-}$ with AngII vehicle (n = 6) each split between 14 and 28 d of

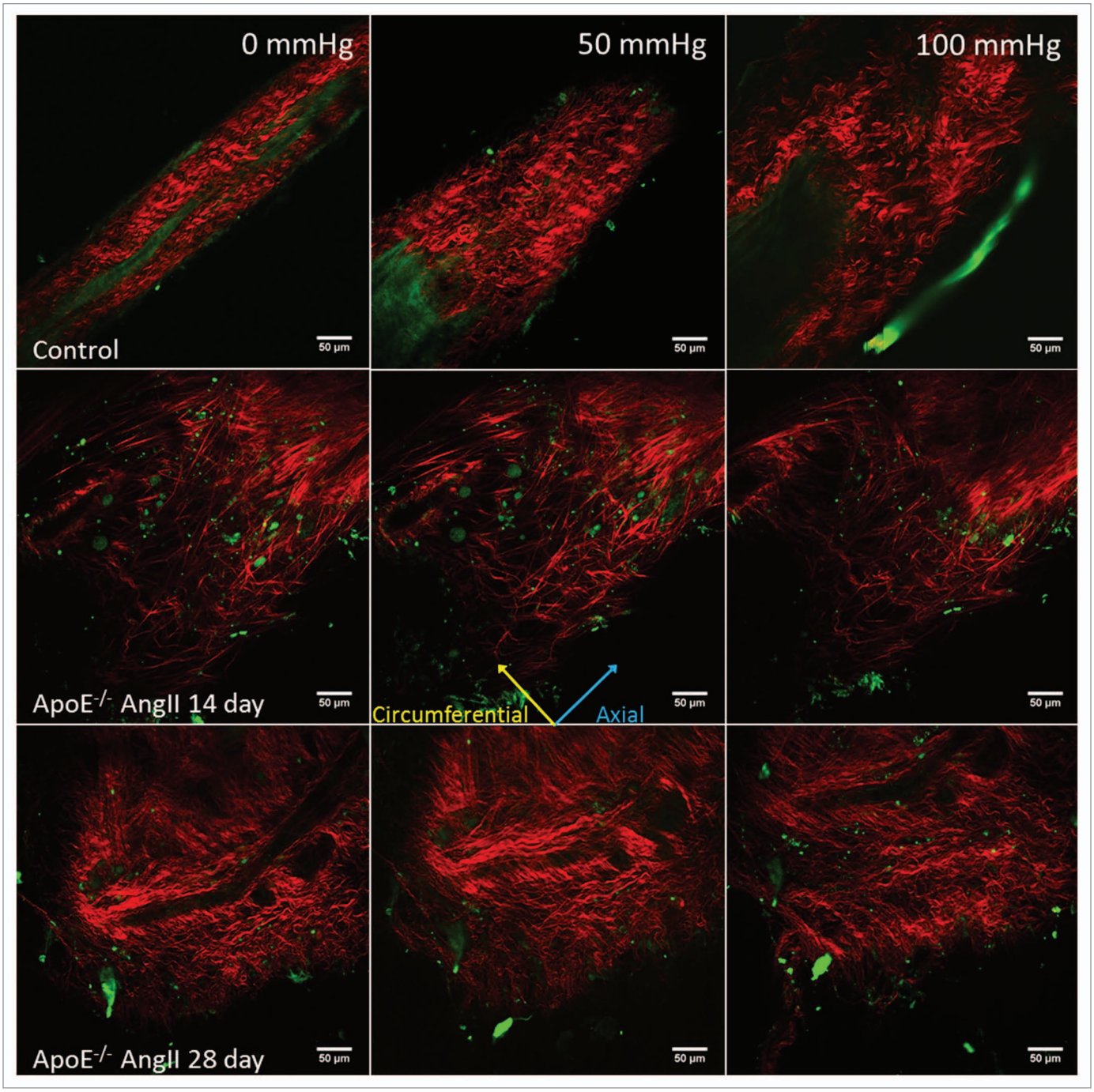

Figure 3. Representative multiphoton images of a control mouse aorta (Top), an AngII infused wild-type mouse (Middle), and ApoE$^{-/-}$ AngII infused model pulled to the in vivo axial strain at both 0 mmHg (Left), 50 mmHg (Middle), and 100 mmHg (RIght). SHG channel (Red) represents the collagen content of the aorta, while NADH channel (Green) represents primarily the elastin content or lipid deposits. While some of elastin bands of the media are observable in the control images, these images are taken approximately in the adventitial layer of the aorta, which was observed to be thicker in both the AngII infused wild-type mouse and the ApoE$^{-/-}$ AngII infused model. Blue and yellow arrows correspond to axial and circumferential directions respectively. In the saline mouse aorta the expected waviness of the collagen fiber bundles is evident in both unpressurized and pressurized states, while both the AngII infused wild-type mouse and the ApoE$^{-/-}$ AngII infused model aortas do not exhibit the expected waviness indicating collagen crimp.

infusion. For the aneurysm model, only specimens that exhibited aneurysm formation (defined as a > 50% increase in aortic diameter or the onset of dissection) and able to undergo full testing at the two time points were used in this study.

At the end of the 14 or 28 d vehicle infusion, mice were sacrificed and the unfixed aorta was isolated and surgically removed (**Fig. 7**) for mechanical testing as reported previously.[12] Briefly, an incision was made from the abdominal cavity to the thoracic

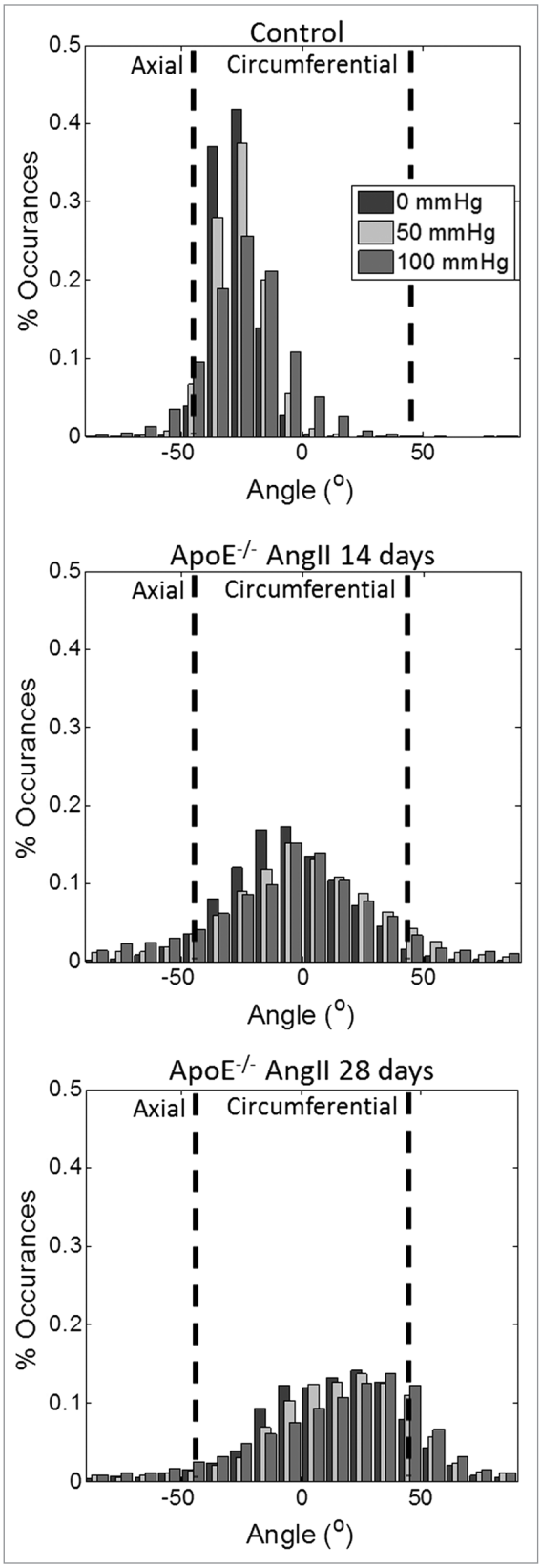

Figure 4. Histogram bars show the overall collagen fiber orientations through the adventitial layer of the aorta at 0 mmHg (Left), 50 mmHg (Middle), and 100 mmHg (Right) pressurized states, with dashed bars representing axial and circumferential directions respectively.

cavity in order to carefully remove the viscera leaving the aorta exposed along the back of the ventral cavity. The physiologic strain was determined using markers placed on the aorta and measured prior to and after excision and detachment. Once excised from the ascending aorta to the iliac bifurcation, the aorta was cleaned of excess perivascular tissue taking care not to damage or tear the specimen. Proximal and distal segments of the vessel were trimmed, and the suprarenal region of the aorta was cannulated onto custom-pulled micropipette capillary tubes and secured using cyanoacrylate adhesive gel. Any large aortic branches were ligated using braided sutures. A small annulus was cut adjacent to the section being tested and imaged to give a mean value for wall thickness photogrammetrically from three averaged measurements.

Mechanical testing and multiphoton imaging protocols. Mechanical testing and imaging protocols have been described previously.[12] Briefly, the specimen was mounted in the tubular-biaxial assembly of our microbiaxial optomechanical device[29] with markers for the strain vision system placed on the vessel. The specimen bath contained PBS, pH-7.4, warmed to 37 ± 0.7°C and was set over the strain vision system. A closed-loop flow system with a syringe pump and pressure transducer controlled luminal pressure within the specimen. A single stepper motor and load cell within the bath allows control of axial displacement and acquisition of axial loads using custom written LabView program (National Instruments). Further details on this device, its capabilities, and its resolutions have been reported previously.[29,30]

For mechanical testing, the original unloaded outer diameter and axial length of the mounted specimen was interactively determined by pulling on the specimen until the point where it no longer bends and creases are not visible in the vessel at zero pressure. The vessel was preconditioned by cycling through axial displacements up to the previously determined physiologic strain with concurrent pressurization of the vessel up to physiologic ranges using 10 consecutive cycles. Biaxial data were collected from a cyclic pressurization test consisting of pressurization from 0 ± 2 mmHg to 100 ± 2 mmHg while stepping through six equal axial displacements up to the physiologic axial strain. Specimens were not inflated or stretched beyond the physiologic values in order to ensure vessel integrity and avoid damage to the ECM that might otherwise occur before imaging. Outputs of the mechanical tests were the vessel radius, axial stretch, lumen pressure and axial load.

Once the mechanical testing was complete the assembly was placed underneath the Advanced Intravital Microscope (AIM) for multiphoton imaging, where the laser power on the sample was 25 mW at an excitation wavelength of λ = 780 nm. Collagen visualization came from second harmonic generation (SHG) collected through a bandpass filter (377/50), while autofluorescence emission from elastin is collected through another bandpass filter (460/80). Further detail on the AIM and the integration of our mechanical device into the AIM can be found in Keyes et al.[31] Each vessel was slowly displaced axially to the physiologic strain used in the mechanical test and held for 3 min to eliminate any viscoelastic effects. Three image

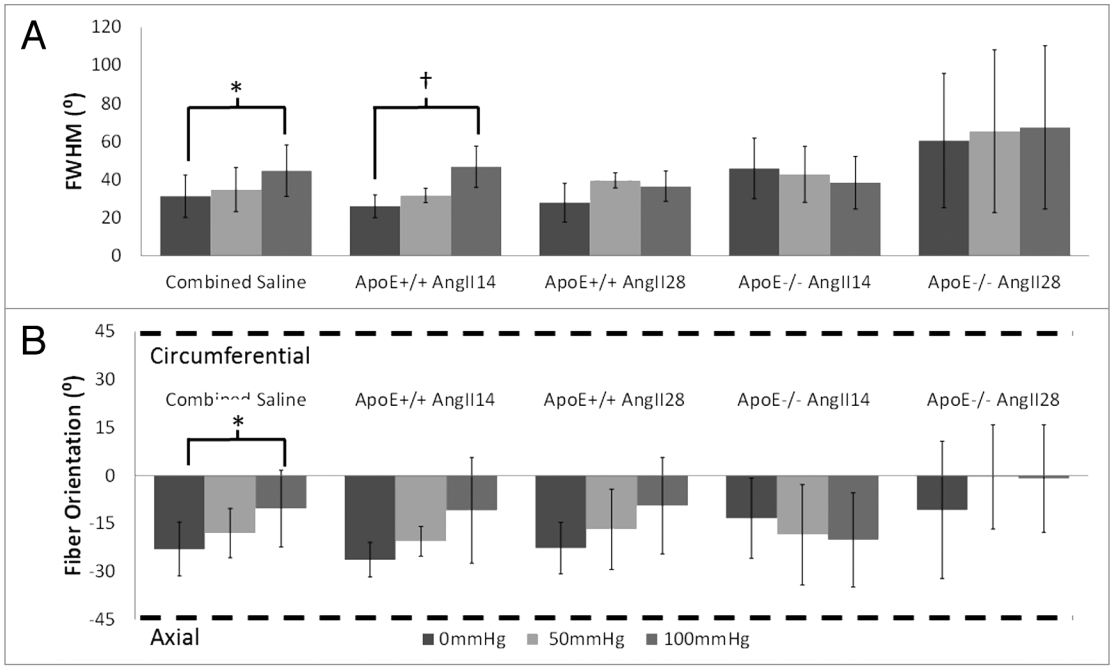

Figure 5. (**A**) The FWHM represents the degree of fiber dispersion, with 0° corresponding fully aligned and 180° corresponding to no fiber alignment or full fiber dispersion. (**B**) The fiber orientation mean mode in reference to −45° being the axial alignment and 45° being circumferential alignment (dashed bars) represents the collagen fibers preferred direction of alignment. Both tiles show the different pressurizations of 0 mmHg (Left), 50 mmHg (Middle), and 100 mmHg (Right). Error bars shown are standard deviation (* $p < 0.05$).

stacks were taken for each specimen, at pressurizations of 0 ± 2, 50 ± 2, 100 ± 2 mmHg, using a 500 × 500 μm field of view at 4 μm steps imaging from the adventitia into the lumen to a depth of 100 μm. Cross-sectional images of the aortas were obtained from vibratoming a portion of the previously mechanically tested to obtain a cross-sectional slice and were again taken using a 500 × 500 μm field of view with 4 μm steps up to a depth of 100 microns. The individual SHG channel was used to determine collagen fiber orientations using a custom written fiber-orientation analysis script for MATLAB (R2013a, MathWorks).[32] Outputs of the image analysis were the mean mode and full width at half max (FWHM), which indicate the preferred fiber alignment and degree of fiber orientation, respectively.

Data analysis and constitutive framework. Data post-processing and constitutive formulation have been described previously.[12] Briefly, the biaxial data were post-processed using MATLAB to give the mean circumferential and axial Cauchy stresses using standard formulae:[23,33-35]

$$\sigma_{\theta\theta} = \frac{P_\theta r_i}{t}, \sigma_{zz} = \frac{P_z}{A} \quad (1)$$

where P_θ is the transluminal pressure, r_i is the deformed (current) inner radius, t is the deformed thickness, P_z is the axial load, and A is the deformed cross-sectional area. The tissue was assumed to be incompressible, and using the previously determined original thickness of the vessel, the deformed cross-sectional area, thickness, and inner radius were determined. Shear components were assumed to be negligible giving the Green strains ($E_{\theta\theta}$, E_{zz}) for both the circumferential and axial directions as[36,37]

$$E_{\theta\theta} = \frac{1}{2}\left(\frac{r^2 - r_o^2}{r_o^2}\right), E_{zz} = \frac{1}{2}(\lambda_z^2 - 1) \quad (2)$$

where r and r_o are the deformed and undeformed mid-thickness radii of the vessel respectively, and λ_z is the axial stretch. For constitutive modeling, the Cauchy stresses were then converted to 2nd Piola Kirchoff stresses ($S_{\theta\theta}$, S_{zz}) determined from the deformation gradient tensor $\mathbf{F}$ and using $\mathbf{S} = J\,\mathbf{F}^{-1}\cdot\boldsymbol{\sigma}\cdot\mathbf{F}^{-1}$, where $J = det\,\mathbf{F} = 1$ for an incompressible material:[19]

$$S_{\theta\theta} = \frac{P_\theta r_i}{t(1+2E_{\theta\theta})}, S_{zz} = \frac{P_z}{A(1+2E_{zz})} \quad (3)$$

We employed a modified form of the Fung strain-energy density function which has been shown to adequately describe the anisotropic mechanical response[37,38] to quantify the biaxial mechanical behavior. The specific form being:

$$W = \frac{C_0}{2}(e^Q - 1), Q = a_1 E_{\theta\theta}^2 + a_2 E_{zz}^2 + 2a_{12} E_{zz} E_{\theta\theta} \quad (4)$$

In this formulation, C_0 is a model parameter associated with initial slope of the mechanical response (having units of stress), and a_1 and a_2 are parameters associated with the circumferential direction ($\theta\theta$) and axial direction (zz) respectively (unitless), and a_{12} is coupling model parameter between the two directions (unitless). Taking the partial derivative of W with respect to $\mathbf{E}$ gives the 2nd Piola Kirchoff stresses for which each specimen was then fit using the constitutive relationship in SigmaStat (v3.1, SPSS) and evaluated to obtain the output metrics of peak strain (defined as the circumferential strain at maximum pressure, i.e., 100 mmHg, and physiologic axial strain) and stiffness (defined as $\partial\mathbf{S}/\partial\mathbf{E}$ at the in vivo axial strain and peak circumferential strain).

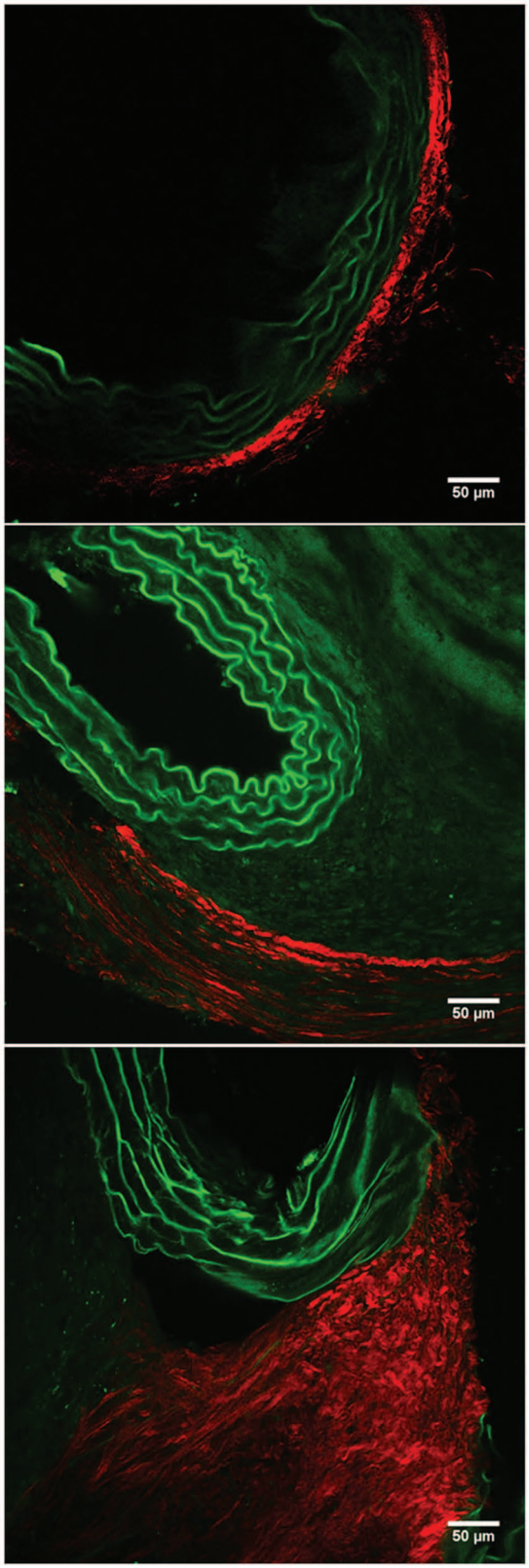

Figure 6. Representative cross-sectional multiphoton images depicting the collagen (red) found in the adventitia and elastin sheets or lipids (green) of the media or dissected aneurysmal sacs for control (top), ApoE$^{-/-}$ AngII infused model at 14 d (middle), and ApoE$^{-/-}$ AngII infused model at 28 d (bottom).

Statistical analysis. A repeated measures analysis of variance (ANOVA) was used to compare across the ApoE$^{-/-}$ AngII infused model, AngII infused wild-type mice, and control groups for each output metric to determine any correlations in changes in mechanical behavior and changes in fiber directionality and dispersion. Pairwise comparisons were performed post hoc to identify which groups were different, with $p < 0.05$ deemed statistically significant. Paired t-tests were used to compare changes within each group for different pressurizations. All statistical analyses were performed in SigmaStat.

Conclusions

In summary, our study, for the first time, quantified biaxial mechanical behavior of the ApoE$^{-/-}$ AngII infused model of aneurysm, while simultaneously quantifying changes in ECM microstructure at multiple time pints. We found that although a reduction in circumferential strain and an increase in circumferential stiffness continued between the 14 and 28 d time points, this was not the case in the axial direction. This return of some of the normal biomechanical function, in addition the continuing changes that occur in the microstructure, suggest a restorative response that occurs in the ApoE$^{-/-}$ AngII infused model after the initial aneurysm formation. Although such finding may cause some reservations about using the ApoE$^{-/-}$ AngII infused aneurysmal model, it might be advantageous to direct future efforts toward understanding and promoting such remodeling, as such a restorative response could have a broader impact on treatments for the human disease. Nevertheless, we hope that the biomechanical material parameters and fiber analysis provided here is able to provide a basis for future work into modeling of aneurysmal progression the ApoE$^{-/-}$ AngII infused model of AAA.

Disclosure of Potential Conflicts of Interest

None of the authors have any conflict of interest.

Acknowledgments

The authors would like to acknowledge the support of the American Heart Association (GIA 10GRNT4580045 to JPVG), the National Science Foundation (CAREER 0644570 to JPVG), the help of Tom Doetschman and Connie Gard, the National Institutes of Health (HL92508), The Stephen Michael Schneider and The William J. "Billy" Gieszl Investigator Award (University of Arizona) and Arizona Biomedical Research Commission (#0901), , and Simmons Clinical Funds, Biomedical Research Grant, Office of the Vice Chancellor of Research, Riley Children Foundation, and the Program for Developmental Biology and Neonatal Medicine at Indiana University College of Medicine (to M.A.).

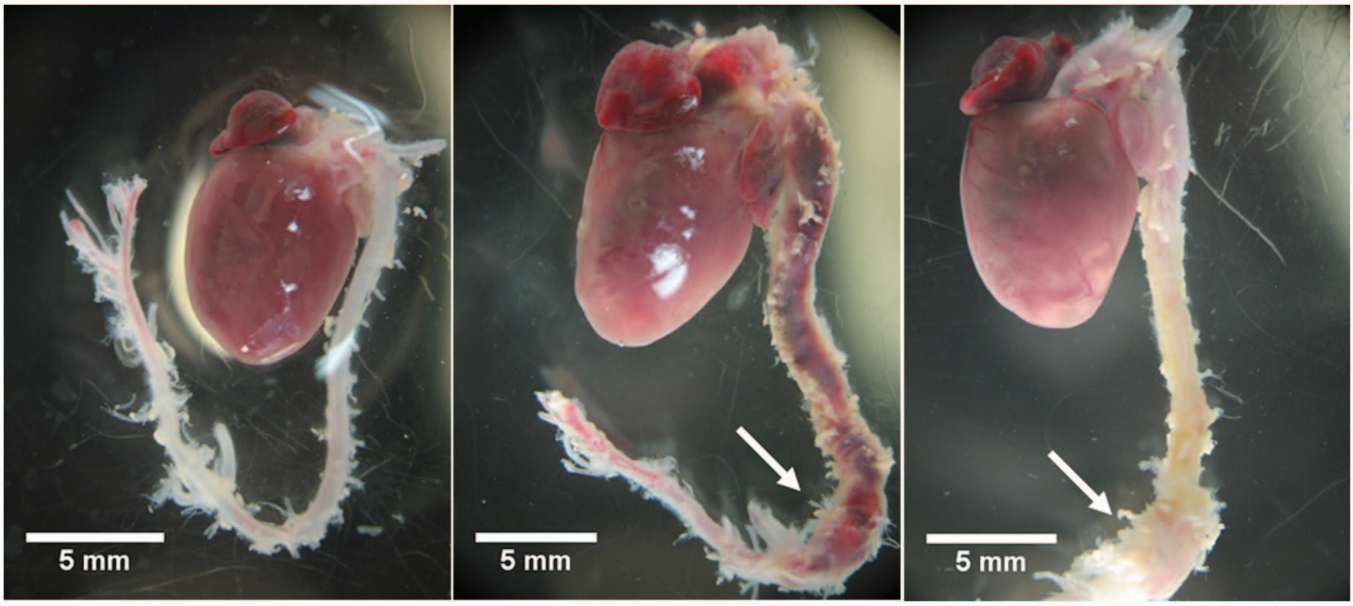

Figure 7. Representative aortas that have been removed and cleaned of excess connective tissue from a control mouse (left), a 14 d ApoE$^{-/-}$ AngII infused aneurysmal mouse (Middle), and a 28 d ApoE$^{-/-}$ AngII infused aneurysmal mouse (right). Arrows indicate an aneurysm in the suprarenal aortic region of the ApoE$^{-/-}$ AngII infused mouse that is absent in the wild-type saline infused mouse.

References

1. Grootenboer N, Bosch JL, Hendriks JM, van Sambeek MR. Epidemiology, aetiology, risk of rupture and treatment of abdominal aortic aneurysms: does sex matter? Eur J Vasc Endovasc Surg 2009; 38:278-84; PMID:19540779; http://dx.doi.org/10.1016/j.ejvs.2009.05.004.
2. Vande Geest JP, Sacks MS, Vorp DA. The effects of aneurysm on the biaxial mechanical behavior of human abdominal aorta. J Biomech 2006; 39:1324-34; PMID:15885699; http://dx.doi.org/10.1016/j.jbiomech.2005.03.003.
3. Vorp DA. Biomechanics of abdominal aortic aneurysm. J Biomech 2007; 40:1887-902; PMID:17254589; http://dx.doi.org/10.1016/j.jbiomech.2006.09.003.
4. Daugherty A, Manning MW, Cassis LA. Angiotensin II promotes atherosclerotic lesions and aneurysms in apolipoprotein E-deficient mice. J Clin Invest 2000; 105:1605-12; PMID:10841519; http://dx.doi.org/10.1172/JCI7818.
5. Hans CP, Koenig SN, Huang N, Cheng J, Beceiro S, Guggilam A, et al. Inhibition of Notch1 signaling reduces abdominal aortic aneurysm in mice by attenuating macrophage-mediated inflammation. Arterioscler Thromb Vasc Biol 2012; 32:3012-23; PMID:23087364; http://dx.doi.org/10.1161/ATVBAHA.112.254219.
6. Iida Y, Xu B, Schultz GM, Chow V, White JJ, Sulaimon S, et al. Efficacy and mechanism of angiotensin II receptor blocker treatment in experimental abdominal aortic aneurysms. PLoS One 2012; 7:e49642; PMID:23226500; http://dx.doi.org/10.1371/journal.pone.0049642.
7. Remus EW, O'Donnell RE Jr., Rafferty K, Weiss D, Joseph G, Csiszar K, et al. The role of lysyl oxidase family members in the stabilization of abdominal aortic aneurysms. Am J Physiol Heart Circ Physiol 2012; 303:H1067-75; PMID:22904155; http://dx.doi.org/10.1152/ajpheart.00217.2012.
8. Yao Y, Wang Y, Zhang Y, Li Y, Sheng Z, Wen S, et al. In vivo imaging of macrophages during the early-stages of abdominal aortic aneurysm using high resolution MRI in ApoE mice. PLoS One 2012; 7:e33523; PMID:22448249; http://dx.doi.org/10.1371/journal.pone.0033523.
9. Ford MD, Black AT, Cao RY, Funk CD, Piomelli U. Hemodynamics of the mouse abdominal aortic aneurysm. J Biomech Eng 2011; 133:121008; PMID:22206425; http://dx.doi.org/10.1115/1.4005477.
10. Goergen CJ, Barr KN, Huynh DT, Eastham-Anderson JR, Choi G, Hedehus M, et al. In vivo quantification of murine aortic cyclic strain, motion, and curvature: implications for abdominal aortic aneurysm growth. J Magn Reson Imaging 2010; 32:847-58; PMID:20882615; http://dx.doi.org/10.1002/jmri.22331.
11. Collins MJ, Bersi M, Wilson E, Humphrey JD. Mechanical properties of suprarenal and infrarenal abdominal aorta: implications for mouse models of aneurysms. Med Eng Phys 2011; 33:1262-9; PMID:21742539; http://dx.doi.org/10.1016/j.medengphy.2011.06.003.
12. Haskett D, Speicher E, Fouts M, Larson D, Azhar M, Utzinger U, et al. The effects of angiotensin II on the coupled microstructural and biomechanical response of C57BL/6 mouse aorta. J Biomech 2012; 45:772-9; PMID:22196971; http://dx.doi.org/10.1016/j.jbiomech.2011.11.017.
13. Fornasa G, Clement M, Groyer E, Gaston AT, Khallou-Laschet J, Morvan M, et al. A CD31-derived peptide prevents angiotensin II-induced atherosclerosis progression and aneurysm formation. Cardiovasc Res 2012; 94:30-7; PMID:22293851; http://dx.doi.org/10.1093/cvr/cvs076.
14. Yang L, Zhou X, Guo R, Shi Y, Liang X, Heng X. Role of Krüppel-like factor 2 and protease-activated receptor-1 in vulnerable plaques of apoe(–/–) mice and intervention with statin. Can J Cardiol 2013; PMID:23395513; http://dx.doi.org/10.1016/j.cjca.2012.11.012.
15. Cassis LA, Gupte M, Thayer S, Zhang X, Charnigo R, Howatt DA, et al. ANG II infusion promotes abdominal aortic aneurysms independent of increased blood pressure in hypercholesterolemic mice. Am J Physiol Heart Circ Physiol 2009; 296:H1660-5; PMID:19252100; http://dx.doi.org/10.1152/ajpheart.00028.2009.
16. Deguchi JO, Huang H, Libby P, Aikawa E, Whittaker P, Sylvan J, et al. Genetically engineered resistance for MMP collagenases promotes abdominal aortic aneurysm formation in mice infused with angiotensin II. Lab Invest 2009; 89:315-26; PMID:19153555; http://dx.doi.org/10.1038/labinvest.2008.167.
17. Sheth RA, Maricevich M, Mahmood U. In vivo optical molecular imaging of matrix metalloproteinase activity in abdominal aortic aneurysms correlates with treatment effects on growth rate. Atherosclerosis 2010; 212:181-7; PMID:20542274; http://dx.doi.org/10.1016/j.atherosclerosis.2010.05.012.
18. Fujikura K, Luo J, Gamarnik V, Pernot M, Fukumoto R, Tilson MD 3rd, et al. A novel noninvasive technique for pulse-wave imaging and characterization of clinically-significant vascular mechanical properties in vivo. Ultrason Imaging 2007; 29:137-54; PMID:18092671; http://dx.doi.org/10.1177/016173460702900301.
19. Vande Geest JP, Sacks MS, Vorp DA. Age dependency of the biaxial biomechanical behavior of human abdominal aorta. J Biomech Eng 2004; 126:815-22; PMID:15796340; http://dx.doi.org/10.1115/1.1824121.
20. Lindeman JH, Ashcroft BA, Beenakker JW, van Es M, Koekkoek NB, Prins FA, et al. Distinct defects in collagen microarchitecture underlie vessel-wall failure in advanced abdominal aneurysms and aneurysms in Marfan syndrome. Proc Natl Acad Sci U S A 2010; 107:862-5; PMID:20080766; http://dx.doi.org/10.1073/pnas.0910312107.
21. Schriefl AJ, Collins MJ, Pierce DM, Holzapfel GA, Niklason LE, Humphrey JD. Remodeling of intramural thrombus and collagen in an Ang-II infusion ApoE$^{-/-}$ model of dissecting aortic aneurysms. Thromb Res 2012; 130:e139-46; PMID:22560850; http://dx.doi.org/10.1016/j.thromres.2012.04.009.

22. Zoumi A, Lu X, Kassab GS, Tromberg BJ. Imaging coronary artery microstructure using second-harmonic and two-photon fluorescence microscopy. Biophys J 2004; 87:2778-86; PMID:15454469; http://dx.doi.org/10.1529/biophysj.104.042887.
23. Eberth JF, Taucer AI, Wilson E, Humphrey JD. Mechanics of carotid arteries in a mouse model of Marfan Syndrome. Ann Biomed Eng 2009; 37:1093-104; PMID:19350391; http://dx.doi.org/10.1007/s10439-009-9686-1.
24. Gasser TC, Ogden RW, Holzapfel GA. Hyperelastic modelling of arterial layers with distributed collagen fibre orientations. J R Soc Interface 2006; 3:15-35; PMID:16849214; http://dx.doi.org/10.1098/rsif.2005.0073.
25. Daugherty A, Rateri DL, Cassis LA. Role of the renin-angiotensin system in the development of abdominal aortic aneurysms in animals and humans. Ann N Y Acad Sci 2006; 1085:82-91; PMID:17182925; http://dx.doi.org/10.1196/annals.1383.035.
26. Saraff K, Babamusta F, Cassis LA, Daugherty A. Aortic dissection precedes formation of aneurysms and atherosclerosis in angiotensin II-infused, apolipoprotein E-deficient mice. Arterioscler Thromb Vasc Biol 2003; 23:1621-6; PMID:12855482; http://dx.doi.org/10.1161/01.ATV.0000085631.76095.64.
27. Barisione C, Charnigo R, Howatt DA, Moorleghen JJ, Rateri DL, Daugherty A. Rapid dilation of the abdominal aorta during infusion of angiotensin II detected by noninvasive high-frequency ultrasonography. J Vasc Surg 2006; 44:372-6; PMID:16890871; http://dx.doi.org/10.1016/j.jvs.2006.04.047.
28. Eagleton MJ, Ballard N, Lynch E, Srivastava SD, Upchurch GR Jr., Stanley JC. Early increased MT1-MMP expression and late MMP-2 and MMP-9 activity during Angiotensin II induced aneurysm formation. J Surg Res 2006; 135:345-51; PMID:16716358; http://dx.doi.org/10.1016/j.jss.2006.03.026.
29. Keyes JT, Haskett DG, Utzinger U, Azhar M, Vande Geest JP. Adaptation of a planar microbiaxial optomechanical device for the tubular biaxial microstructural and macroscopic characterization of small vascular tissues. J Biomech Eng 2011; 133:075001; PMID:21823753; http://dx.doi.org/10.1115/1.4004495.
30. Keyes JT, Borowicz SM, Rader JH, Utzinger U, Azhar M, Vande Geest JP. Design and demonstration of a microbiaxial optomechanical device for multiscale characterization of soft biological tissues with two-photon microscopy. Microsc Microanal 2011; 17:167-75; PMID:21226989; http://dx.doi.org/10.1017/S1431927610094341.
31. Keyes JT, Borowicz SM, Rader JH, Utzinger U, Azhar M, Vande Geest JP. Design and demonstration of a microbiaxial optomechanical device for multiscale characterization of soft biological tissues with two-photon microscopy. Microsc Microanal 2011; 17:167-75; PMID:21226989; http://dx.doi.org/10.1017/S1431927610094341.
32. Kirkpatrick ND, Hoying JB, Botting SK, Weiss JA, Utzinger U. In vitro model for endogenous optical signatures of collagen. J Biomed Opt 2006; 11:054021; PMID:17092170; http://dx.doi.org/10.1117/1.2360516.
33. Schulze-Bauer CA, Regitnig P, Holzapfel GA. Mechanics of the human femoral adventitia including the high-pressure response. Am J Physiol Heart Circ Physiol 2002; 282:H2427-40; PMID:12003855.
34. Gleason RL, Wilson E, Humphrey JD. Biaxial biomechanical adaptations of mouse carotid arteries cultured at altered axial extension. J Biomech 2007; 40:766-76; PMID:16750537; http://dx.doi.org/10.1016/j.jbiomech.2006.03.018.
35. Humphrey JD, Eberth JF, Dye WW, Gleason RL. Fundamental role of axial stress in compensatory adaptations by arteries. J Biomech 2009; 42:1-8; PMID:19070860; http://dx.doi.org/10.1016/j.jbiomech.2008.11.011.
36. Debes JC, Fung YC. Biaxial mechanics of excised canine pulmonary arteries. Am J Physiol 1995; 269:H433-42; PMID:7653607.
37. Fung Y. *Biomechanics: Mechanical properties of living tissues*. New York: Springer; 1993.
38. Fung YC, Liu SQ. Determination of the mechanical properties of the different layers of blood vessels in vivo. Proc Natl Acad Sci U S A 1995; 92:2169-73; PMID:7892241; http://dx.doi.org/10.1073/pnas.92.6.2169.